eNeuro

Research Article: New Research

Development

Using SuperClomeleon to Measure Changes in Intracellular Chloride during Development and after Early Life Stress

Lotte J. Herstel,[1,*] Carlijn Peerboom,[1,*] Sten Uijtewaal,[1] Dunya Selemangel,[1] Henk Karst,[2] and Corette J. Wierenga[1]

https://doi.org/10.1523/ENEURO.0416-22.2022

[1]Cell Biology, Neurobiology and Biophysics, Biology Department, Utrecht University, 3584 CH, Utrecht, The Netherlands and [2]Utrecht Brain Center, University Medical Center Utrecht, 3584 CX, Utrecht, The Netherlands

Abstract

Intraneuronal chloride concentrations ($[Cl^-]_i$) decrease during development resulting in a shift from depolarizing to hyperpolarizing GABA responses via chloride-permeable $GABA_A$ receptors. This GABA shift plays a pivotal role in postnatal brain development, and can be strongly influenced by early life experience. Here, we assessed the applicability of the recently developed fluorescent SuperClomeleon (SClm) sensor to examine changes in $[Cl^-]_i$ using two-photon microscopy in brain slices. We used SClm mice of both sexes to monitor the developmental decrease in neuronal chloride levels in organotypic hippocampal cultures. We could discern a clear reduction in $[Cl^-]_i$ between day *in vitro* (DIV)3 and DIV9 (equivalent to the second postnatal week *in vivo*) and a further decrease in some cells until DIV22. In addition, we assessed alterations in $[Cl^-]_i$ in the medial prefrontal cortex (mPFC) of postnatal day (P)9 male SClm mouse pups after early life stress (ELS). ELS was induced by limiting nesting material between P2 and P9. ELS induced a shift toward higher (i.e., immature) chloride levels in layer 2/3 cells in the mPFC. Although conversion from SClm fluorescence to absolute chloride concentrations proved difficult, our study underscores that the SClm sensor is a powerful tool to measure physiological changes in $[Cl^-]_i$ in brain slices.

Key words: chloride; FRET sensor; GABA shift; two-photon microscopy

Significance Statement

The reduction of intraneuronal chloride concentrations is crucial for brain development, as it ensures a shift from the initial excitatory action of the neurotransmitter GABA in immature neurons to the inhibitory GABA signaling in the adult brain. Recent development of chloride sensors enable direct imaging of intracellular chloride signaling in neurons. Here, we assessed the applicability of the SuperClomeleon (SClm) chloride sensor to measure physiologically relevant changes in chloride levels using two-photon microscopy in cultured and acute brain slices. Although we also point out some limitations, we conclude that the SuperClomeleon sensor is a powerful tool to measure physiological changes in intracellular chloride.

Introduction

During normal neuronal development, GABA responses through ionotropic $GABA_A$ receptors shift from depolarizing to hyperpolarizing as a result of the developmental decrease in intracellular chloride concentration. In the immature brain, the intracellular chloride concentration is high and activation of $GABA_A$ receptors results in an outflow of chloride leading to membrane depolarization. During early postnatal development, intracellular chloride

Received October 5, 2022; accepted November 30, 2022; First published December 7, 2022.
The authors declare no competing financial interests.

Author contributions: L.J.H., C.P., and C.J.W. designed research; L.J.H. and C.P. performed research; H.K. contributed unpublished reagents/analytic tools; L.J.H., C.P., S.U., and D.S. analyzed data; L.J.H., C.P., and C.J.W. wrote the paper.

levels gradually decrease. As a result, activation of $GABA_A$ receptors in mature neurons leads to the influx of chloride and GABAergic signaling induces membrane hyperpolarization (Rivera et al., 1999; Ben-Ari et al., 2007; Kaila et al., 2014). This shift in GABA signaling plays a pivotal role in postnatal neuronal development and its timing affects brain function throughout life (Sernagor et al., 2010; Kaila et al., 2014; Lohmann and Kessels, 2014; Peerboom and Wierenga, 2021).

In rodents the GABA shift occurs normally between postnatal day (P)10 and P14 depending on brain region and cell type (Rivera et al., 1999; Stein et al., 2004; Ben-Ari et al., 2007; Romo-Parra et al., 2008; Glykys et al., 2009; Kirmse et al., 2015; Sulis Sato et al., 2017). For example, intracellular chloride levels in the visual cortex mature several days earlier compared with the hippocampus (Murata and Colonnese, 2020), while in the prefrontal cortex (PFC) the GABA shift occurs even later (Amadeo et al., 2018; Karst et al., 2019). In addition, GABAergic maturation has been shown to be strongly influenced by experiences during early life. For instance, prenatal maternal restraint stress as well as repeated separations of newborn pups from their mother induced a delay in the GABA shift in hippocampal pyramidal cells in young mice (Veerawatananan et al., 2016; Furukawa et al., 2017; Hu et al., 2017). Early life stress (ELS) has life-long consequences on neurophysiology and behavior in both humans and rodents and poses an increased risk for psychopathology later in life (Teicher et al., 2016; Joëls et al., 2018). The medial prefrontal cortex (mPFC) is known to be very sensitive to stress early in life, with life-long consequences for anxiety and stress responses (Ishikawa et al., 2015; Karst et al., 2020). The mPFC functions as a central coordinator of stress responses across brain regions as well as the periphery (McKlveen et al., 2015). However, it is currently unclear how GABA signaling in the mPFC is affected by ELS.

In most studies, intracellular chloride concentrations in neurons are determined using perforated patch clamp recordings. With this technique antibiotics (e.g., gramicidin or amphotericin B) are included in the pipette to form small pores in the membrane which leaves intracellular chloride concentration intact. However, perforated patch clamp recordings are time intensive and it is difficult to perform long recordings, as access is not stable (Arosio et al., 2010). Large individual differences can exist between neurons and many individual recordings may be required to get a good population estimate (Tyzio et al., 2007; Sulis Sato et al., 2017). As a promising alternative, biosensors are being developed which allow for the real time measurement of intracellular chloride levels in a noninvasive manner (Arosio et al., 2010). The SuperClomeleon (SClm) sensor (Grimley et al., 2013) is a second generation chloride sensor with chloride sensitivity in the physiological range. The SClm sensor consists of two fluorescent proteins, Cerulean (CFP mutant) and Topaz (YFP mutant), joined by a flexible linker. Depending on the binding of chloride, Fluorescence Resonance Energy Transfer (FRET) occurs from the CFP donor to the YFP acceptor (Grimley et al., 2013). FRET ratios (fluorescence intensity of YFP/CFP) are independent of expression level and imaging settings, which is a major advantage when imaging in intact brain tissue. The SClm sensor has successfully been used to determine the steady-state intracellular chloride concentration in adult mice *in vivo* (Boffi et al., 2018) and to demonstrate the existence of cytoplasmic chloride microdomains in neurons (Rahmati et al., 2021), but it has not been used to examine chloride maturation during neuronal development.

Here, we used the SClm sensor to detect changes in chloride during early postnatal development in organotypic hippocampal cultures of mice and in acute slices of the prefrontal cortex from young control mice and mice who experienced ELS.

Materials and Methods

Animals

SuperClomeleon$^{lox/-}$ mice (Rahmati et al., 2021; a gift from Kevin Staley, Massachusetts General Hospital, Boston, MA) were crossed with CamKII$\alpha^{Cre/-}$ mice (Casanova et al., 2001; Tsien et al., 1996; a gift from Stefan Berger, German Cancer Research Center, Heidelberg, Germany) and will hereafter be referred to as SClm mice. Animals were housed at reversed day-night cycle with a room temperature of 22 ± 2°C and humidity of ~65%. Food (standard chow) and water were provided *ad libitum*. We noticed that SClm mice had poor breeding performance compared with other strains kept in the same facility. On postnatal day (P)2 the litter was randomly assigned to either the control condition (standard housing) or the ELS condition. In the ELS condition a limited amount of nesting and bedding material was made available between P2 and P9 (Rice et al., 2008; Naninck et al., 2015; Karst et al., 2020). All animal experiments were performed in compliance with the guidelines for the welfare of experimental animals and were approved by the local authorities.

Organotypic culture preparation

Postnatal developmental changes in intracellular chloride concentration ($[Cl^-]_i$) were imaged in organotypic hippocampal cultures made from P6 control SClm mice of both sexes. For the chloride calibration and wash-in experiments, organotypic hippocampal cultures were made

This work was supported by the ZonMW TOP Grant 9126021, the Foundation for Fundamental Research on Matter (FOM) Research Program Grant 16NEPH05, and the Dutch Research Council (NWO) Open Competition Program Grant OCENW.KLEIN.150.

Acknowledgments: We thank Prof. Kevin Staley for providing the SuperClomeleon$^{lox/-}$ mouse line and SClm AAV and Dr. Stefan Berger for the CamKII$\alpha^{Cre/-}$ mice; several members of the Staley lab for helpful discussions; René van Dorland for his technical support with the AAV; and Prof. Marian Joëls for her constructive feedback on this manuscript.

*L.J.H. and C.P. contributed equally to this work.

C. J. Wierenga's present address: Faculty of Science and Donders Institute, Radboud University, Nijmegen, The Netherlands.

Correspondence should be addressed to C. J. Wierenga at corette.wierenga@donders.ru.nl.

https://doi.org/10.1523/ENEURO.0416-22.2022

from P6 wild-type (WT) C57BL/6 mice and SCIm expression was achieved by viral injection. Slice cultures were prepared using a method based on Stoppini et al. (1991). After decapitation the brain was rapidly removed and placed in ice-cold Gey's balanced salt solution [GBSS; containing (in mM): 137 NaCl, 5 KCl, 1.5 $CaCl_2$, 1 $MgCl_2$, 0.3 $MgSO_4$, 0.2 KH_2PO_4, and 0.85 Na_2HPO_4] with 25 mM glucose, 12.5 mM HEPES, and 1 mM kynurenic acid. Transverse hippocampal slices of 400 μm thick were cut with a McIlwain tissue chopper (Brinkmann Instruments). Slices were placed on Millicell membrane inserts (Millipore) in wells containing 1-ml culture medium (consisting of 48% MEM, 25% HBSS, 25% horse serum, 25 mM glucose, and 12.5 mM HEPES, with an osmolarity of 325 mOsm and a pH of 7.3–7.4). Slices were stored in an incubator (35°C with 5% CO_2) and medium was replaced three times a week. Experiments were performed after 1–22 d *in vitro* (DIV).

Viral expression

An adeno-associated virus (AAV) with Cre-independent expression of SCIm under the control of the Synapsin promotor (AAV9.hSyn.sCLM; a gift from Kevin Staley, Massachusetts General Hospital, Boston, MA) was injected in the CA1 area of WT cultured hippocampal slices on DIV1. Slices were imaged on DIV9–16. Compared with slices from SCIm mice, viral expression of the SCIm sensor resulted in larger variability in neuronal FRET (YFP/CFP) ratios, probably because of variability in slice quality and viral expression levels. We optimized the viral concentration to get comparable levels of YFP and CFP fluorescent intensity as observed in the mouse line.

Acute slice preparation

Young SCIm mice were decapitated at P9, followed by quick removal of the brain. For this study we used only male mice to allow direct comparison with our earlier study in C57/BL6 mice (Karst et al., 2019). Mice were always decapitated in the morning to eliminate influences of fluctuating corticosterone (CORT) levels during the day, because of the reversed day-night cycle this means that CORT levels are high at that time. The brain was stored in ice cold artificial CSF [ACSF; containing (in mM): 120 choline chloride, 3.5 KCl, 0.5 $CaCl_2$, 6 $MgSO_4$, 1.25 NaH_2PO_4, 25 D-glucose, and 25 $NaHCO_3$]. Coronal slices of 350 μm thickness were made with a vibratome (Leica VT 1000S). After placing them in ACSF [consisting of (in mM): 120 NaCl, 3.5 KCl, 1.3 $MgSO_4$, 1.25 NaH_2PO_4, 2.5 $CaCl_2$, 25 D-glucose, and 25 $NaHCO_3$] slices were heat shocked at 32°C for 20 min. Slices were then kept at room temperature and after recovery for at least 1 h, transported individually in Eppendorf tubes filled with ACSF to the microscope room in another building with a transportation time of 10 min.

Two-photon imaging

Slices were transferred to the microscope chamber. The bath was continuously perfused with carbonated (95% O_2, 5% CO_2) ACSF (in mM: 126 NaCl, 3 KCl, 2.5 $CaCl_2$, 1.3 $MgCl_2$, 26 $NaHCO_3$, 1.25 NaH_2PO_4, 20 D-glucose, and 1 Trolox, with an osmolarity of 310 $\pm$ 10 mOsm/l) at a rate of $\sim$1 ml/min. Bath temperature was monitored and maintained at 30–32°C throughout the experiment. Two-photon imaging of pyramidal neurons in layer 2/3 of the mPFC or pyramidal neurons in the CA1 area of the hippocampus was performed on a customized two-photon laser scanning microscope (Femto3D-RC, Femtonics). To excite the CFP donor, a Ti-Sapphire femtosecond pulsed laser (MaiTai HP, Spectra-Physics) was tuned to 840 nm. The emission signal was split using a dichroic beam splitter at 505 nm and detected using two GaAsP photomultiplier tubes. We collected fluorescence emission of Cerulean/CFP (485 $\pm$ 15 nm) and Topaz/YFP (535 $\pm$ 15 nm) in parallel. A 60$\times$ water immersion objective (Nikon NIR Apochromat; NA 1.0) was used to locate the cell layer. Of each slice, two to four image z-stacks in different field of views (FOV) were acquired at a resolution of 8.1 pixels/μm (1024 $\times$ 1024 pixels, 126 $\times$ 126 μm) with 1-μm steps of $\sim$40–85 μm in depth. To monitor acute changes in $[Cl^-]_i$ we bath applied $GABA_A$ receptor agonist muscimol (Tocris, 10 μM) and imaged at lower resolution [every 2 min at a resolution of 4.1 pixels/μm (512 $\times$ 512 pixels, 126 $\times$ 126 μm) with 1-μm steps of 30–50 μm in depth].

Imaging data analysis

Image analysis was performed using Fiji/ImageJ software and results were analyzed in Prism 9 (GraphPad). We manually determined regions of interest (ROIs) around individual neuron somata. To analyze a representative cell population, in each image z-stack we selected four z-planes at comparable depths in which three cells were identified that varied in brightness (bright, middle and dark). We subtracted the mean fluorescence intensity of the background in the same image plane from the mean fluorescence intensity of CFP and YFP before calculating the fluorescence ratio. We limited our analysis to cells which were located within 450 pixels from the center of the image, as FRET ratios showed slight aberrations at the edge of our images. We excluded cells with a FRET ratio $<$0.5 or $>$1.6, to avoid the selection of unhealthy cells (59 of 1893 cells; 3.1%). We verified that inclusion of these cells did not change our conclusions. We confirmed that the FRET ratios of individual cells were uncorrelated with their fluorescence intensities (data not shown).

FRET-colored images (as shown in Figs. 1*C*, 2*D*, 3*A*, 4*A*) were made in ImageJ. We first subtracted the average background and Gaussian filtered the CFP and YFP image z-stacks separately. Next, the acceptor (YFP) image was divided by the donor (CFP) image to get the ratiometric image. A mask was created by manually drawing ROIs for each soma in the image. An average projection of the radiometric image was made of a specific z range and multiplied by the mask. Finally, the masked ratiometric image was combined with the grayscale image. Please note that these images were made for illustration purposes only, analysis was performed on the raw data.

SCIm sensor calibration

Calibrations for chloride were performed as described before (Grimley et al., 2013; Boffi et al., 2018; Rahmati et

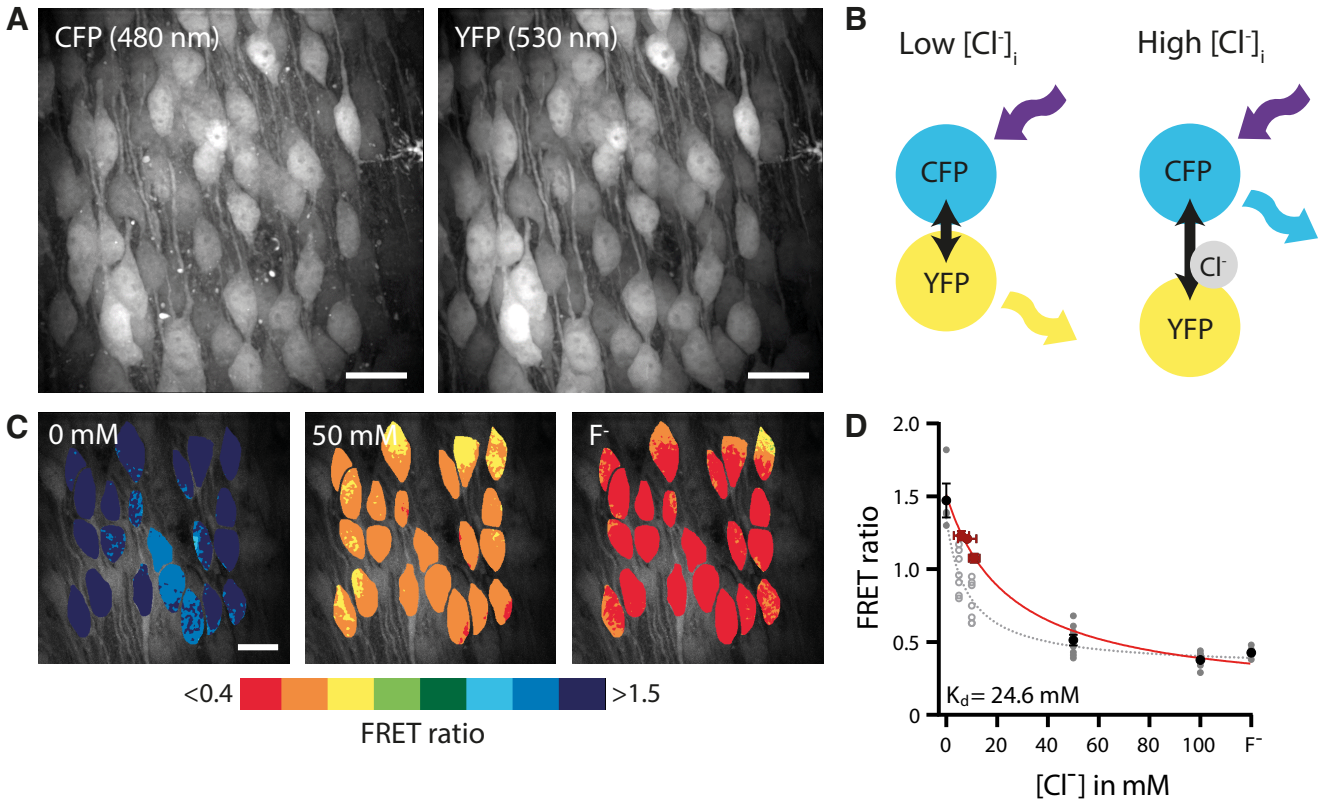

Figure 1. Two-photon imaging of $[Cl^-]_i$ in brain slices. ***A***, Example image of CFP (480 nm) and YFP (530 nm) fluorescence in an organotypic hippocampal culture from a SCIm mouse. Scale bar: 20 μm. ***B***, Illustration of Fluorescence Resonance Energy Transfer (FRET) from CFP donor to YFP acceptor of the SCIm sensor. FRET values (YFP/CFP fluorescence ratio) decrease with higher chloride concentrations. ***C***, Two-photon imaging of chloride-dependent changes in the FRET ratio (530/480-nm emission) in a WT organotypic hippocampal culture with AAV SCIm expression. $[Cl^-]_i$ was clamped to the indicated external chloride concentration via ionophore treatment. Individual cells are color-coded to their FRET ratios. Scale bar: 20 μm. ***D***, Calibration curve constructed from ionophore experiments (black/gray symbols) and perforated patch (red symbols) data. Data are presented as mean ± SEM. These data were fit by Equation 2, yielding the following fit parameters: K_d = 24.6 mM, R_{max} = 1.51, R_{min} = 0.12 (red curve; for details, see Materials and Methods). This calibration curve was used to convert FRET ratios into estimated chloride levels in the rest of this study. We also show the individual data points representing individual ionophore experiments (average over 12 cells per experiment). At 5 and 10 mM extracellular chloride FRET values were highly variable (open symbols). As described in Materials and Methods, we excluded these data points from our analysis and resorted to perforated patch recordings (red symbols) for this chloride range. The gray dotted line shows the alternative calibration curve when all ionophore data are included (fit parameters K_d = 8.4; R_{max} = 1.35; R_{min} = 0.32; without perforated patch data). Electrophysiology data from 11 cells (DIV1–3), 9 cells (DIV8–10), and 13 cells (DIV20–22); SCIm data from 11 slices.

al., 2021). As SCIm mice were no longer available we used organotypic hippocampal cultures from WT mice expressing the SCIm sensor. Cultured slices were treated with ionophores (100 μM nigericin and 50 μM tributyltin acetate, Merck) to clamp $[Cl^-]_i$ and intracellular pH to extracellular levels. Saline containing various $[Cl^-]_i$ were perfused at ~1 ml/min. High chloride solution consisted of (in mM): 105 KCl, 48 NaCl, 10 HEPES, 20 D-glucose, 2 Na-EGTA, and 4 $MgCl_2$, whereas the solution without chloride contained (in mM): 105 K-gluconate, 48 Na-gluconate, 10 HEPES, 20 D-glucose, 2 Na-EGTA, and 4 $Mg(gluconate)_2$. The high extracellular K^+ concentrations are necessary for proper functioning of nigericin (Pressman and Fahim, 1982). Intermediate $[Cl^-]_i$ solutions (0, 5, 10, 50, and 100 mM) were prepared by mixing the two solutions. To maximally quench the SCIm sensor we used a KF solution containing (in mM): 105 KF, 48 NaF, 10 HEPES, 20 D-glucose, 2 Na-EGTA, and 4 $Mg(gluconate)_2$. All calibration solutions were adjusted to pH 7.4. The first calibration solution with ionophores was washed in for 20 min and subsequent calibration solutions with ionophores were washed in for 15 min. Image z-stacks were acquired every 3 min at a resolution of 4.1 pixels/μm (512 × 512 pixels, 126 × 126 μm) with 1-μm steps of 30–50 μm in depth. FRET ratios reached a plateau after 10 min of wash in, which we assumed reflected equal intracellular and extracellular chloride concentrations. We constructed the calibration curve by plotting measured FRET ratios against extracellular chloride concentrations.

However, we noticed that FRET ratios differed widely between experiments, especially at intermediate chloride levels (5–10 mM). As this severely impaired robustness o the calibration in the most relevant chloride range, we resorted to perforated patch clamp measurements to

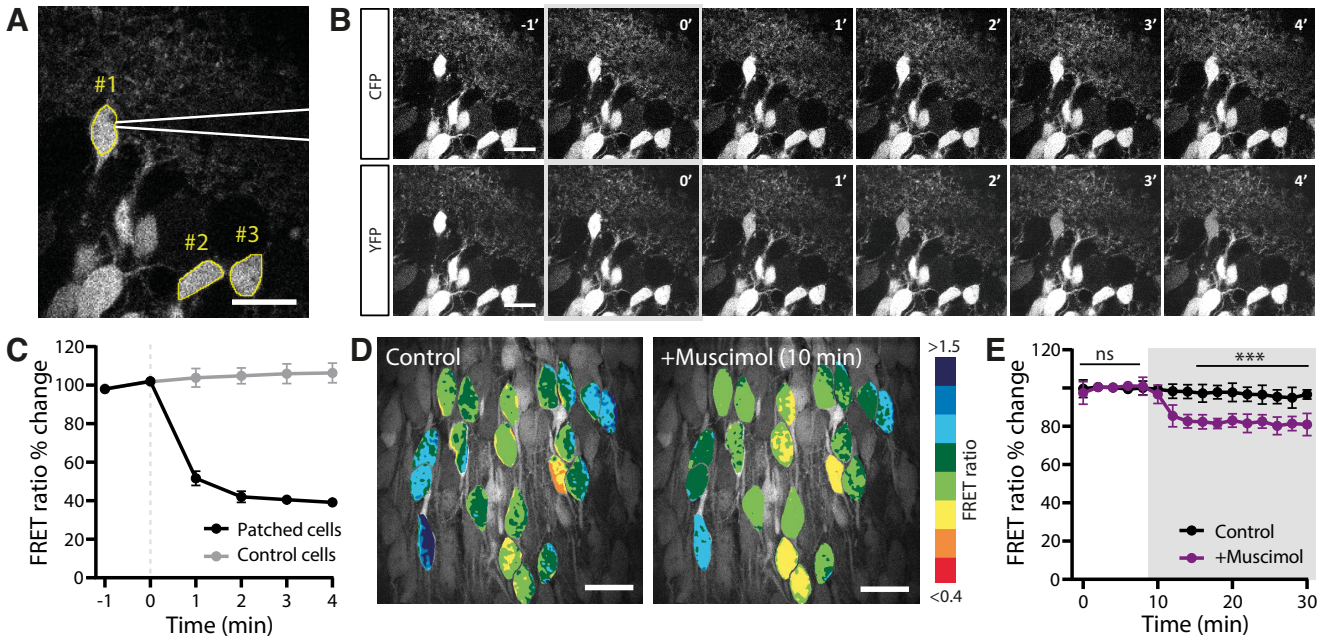

Figure 2. Monitoring acute changes in $[Cl^-]_i$ with SClm. ***A***, Two-photon image of CA1 pyramidal neurons in the hippocampus of an acute slice from a SClm mouse. A patch pipette (in white) is attached to cell #1 for a whole-cell recording. Two control cells are indicated with #2 and #3. Scale bar: 20 μm. ***B***, Time course of CFP (upper row) and YFP (lower row) fluorescence right before and during the first minutes after break-in. After break-in (0'; gray) cell #1 rapidly fills with the high chloride internal solution (70 mM KCl) resulting in a decrease in YFP fluorescence. Scale bar: 20 μm. ***C***, Average FRET ratio over time for cells that were infused with 70 mM KCl ($n = 2$), and neighboring control cells ($n = 4$). Error bars represents SEM. ***D***, Acute wash-in with muscimol in cultured slices with viral SClm expression caused a decrease in FRET ratio in CA1 pyramidal neurons within 10 min. Scale bar: 20 μm. ***E***, Average FRET ratios over time during wash-in of muscimol (gray area) and control. Data from 84 cells, 7 slices, 4 mice in both groups.

calibrate the SClm sensor within the physiological range. We performed perforated patch clamp recordings in organotypic hippocampal cultures to determine $[Cl^-]_i$ in CA1 pyramidal cells at DIV1–3, DIV8–10, and DIV20–22 (described below). We plotted the average $[Cl^-]_i$ values against the average FRET ratios measured in cells at the same DIVs and added these data to the calibration data from the ionophores. We fitted this composite calibration curve (Fig. 1*D*) with the following relation between FRET ratios and $[Cl^-]_i$ (Grimley et al., 2013; Boffi et al., 2018; Rahmati et al., 2021):

$$[Cl^-]_i = K_d * \left(\frac{R_{max} - R}{R - R_{min}}\right), \quad (1)$$

(in which R is the YFP/CFP emission ratio), to obtain the dissociation constant K_d and the minimum and maximum FRET ratio R_{min} and R_{max} for our measurements.

Electrophysiology

Whole-cell patch clamp recordings were made of pyramidal neurons in the hippocampal CA1 or mPFC of acute slices from SClm mice. Recording pipettes (resistance of 4–6 MΩ) were pulled from thick-walled borosilicate glass capillaries (World Precision Instruments) and filled with high chloride internal solution (in mM: 70 K-gluconate, 70 KCl, 0.5 EGTA, 10 HEPES, 4 MgATP, 0.4 NaGTP, and 4 Na_2-phosphocreatine with pH 7.3 and osmolarity 295 mOsm/l). Cells were kept at a holding potential of −60 mV in voltage clamp throughout the experiment.

Perforated patch clamp recordings were made from CA1 pyramidal neurons in cultured hippocampal slices from WT mice at 30–32°C. Recording pipettes (resistance of 2–4 MΩ) were pulled from thick-walled borosilicate glass capillaries (World Precision Instruments). The pipette tip was filled with gramicidin-free KCl solution (140 mM KCl and 10 mM HEPES, pH 7.2, and osmolarity 285 mOsm/L) and then backfilled with the KCl solution containing gramicidin (60 μg/ml, Sigma). CA1 neurons were clamped at −65 mV and the access resistance of the perforated cells was monitored constantly before and during recordings. An access resistance of 50 MΩ was considered acceptable to start recording. GABAergic currents were evoked by puffs of 50 μM muscimol (Tocris) dissolved in HEPES-buffered ACSF (in mM: 135 NaCl, 3 KCl, 2.5 $CaCl_2$, 1.3 $MgCl_2$, 1.25 $Na_2H_2PO_4$, 20 glucose, and 10 HEPES) in the presence of 1 μM TTX (Abcam). To determine the reversal potential of chloride, GABAergic currents were recorded at a holding potentials between −100 and −30 mV in 10-mV steps, on local somatic application of the $GABA_A$ receptor agonist muscimol (50 μM) dissolved in HEPES-buffered ACSF every 30 s using a Picospritzer II. The GABA reversal potential was determined from the intersection of the current–voltage curve with the x-axis. We assumed that the chloride reversal

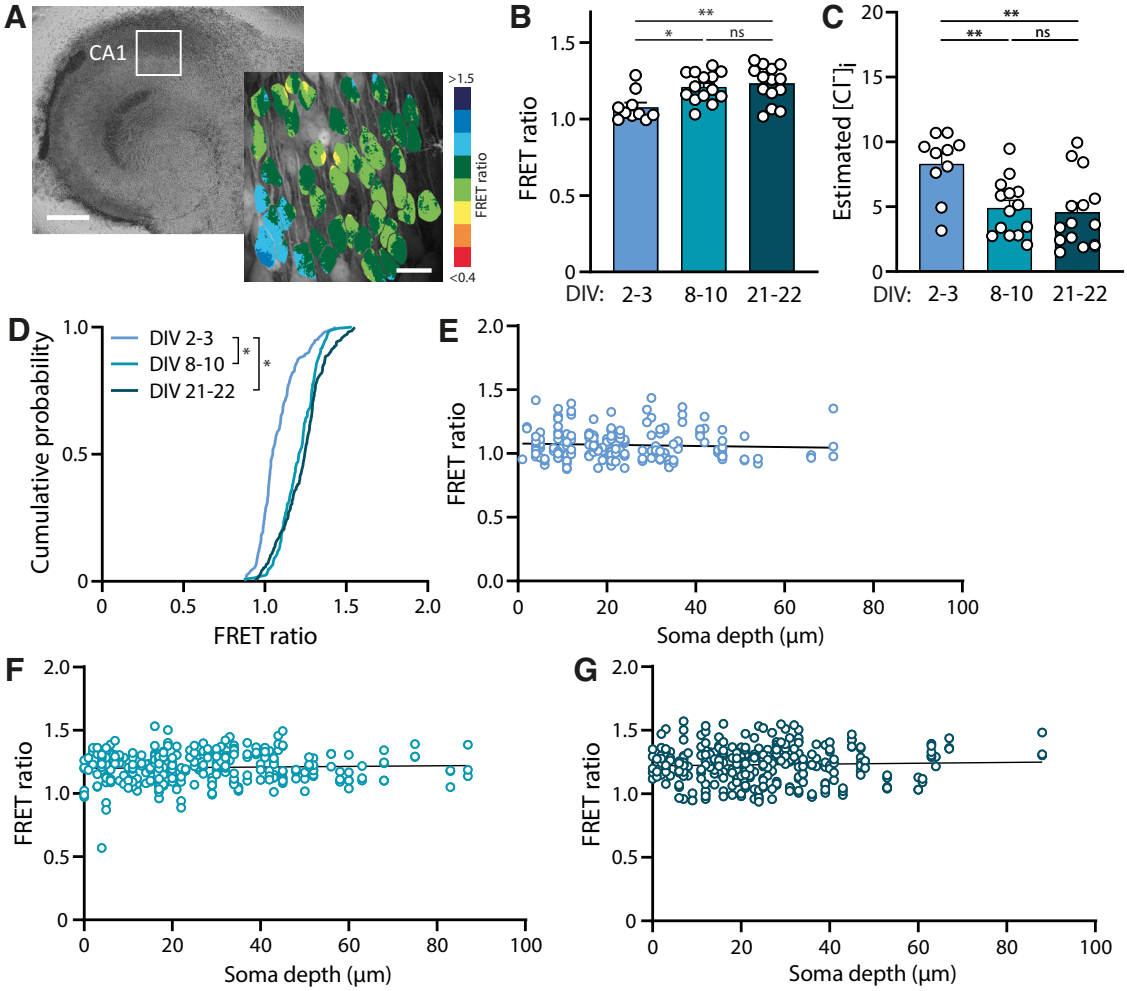

Figure 3. Developmental decrease in $[Cl^-]_i$ continues in organotypic cultures. ***A***, Example of an organotypic hippocampal culture from a SClm mouse at DIV8. Scale bar: 500 µm. In the zoom an example of the FRET ratios determined in the CA1 area. Scale bar: 20 µm. ***B***, Average FRET ratios of CA1 pyramidal cells at DIV2–3 ($n = 10$ slices of 6 mice), DIV8–10 ($n = 14$ slices of 8 mice), and DIV21–22 ($n = 14$ slices of 8 mice). There was a significant increase in FRET ratio over time ($p = 0.033$ DIV2–3 vs DIV8–10; $p = 0.008$ DIV2–3 vs DIV21–22; $p > 0.99$ DIV8–10 vs DIV21–22; KW test). ***C***, Average estimated $[Cl^-]_i$ as calculated from the FRET ratios in ***B***. There was a significant decrease in $[Cl^-]_i$ over time ($p = 0.006$ DIV2–3 vs DIV8–10; $p = 0.003$ DIV2–3 vs DIV21–22; $p = 0.93$ DIV8–10 vs DIV21–22; one-way ANOVA). ***D***, Cumulative distribution of FRET ratios for individual cells at the three time points. For each slice, 15 cells were randomly selected, making the total of number of plotted cells per condition at least 150 ($p < 0.001$ DIV2–3 vs DIV8–10 and vs DIV21–22; $p = 0.053$ DIV8–10 vs DIV21–22; KS test). ***E***, Individual FRET ratios plotted against soma depth in slices at DIV2–3 ($n = 186$ neurons). Line represents linear regression fit ($r = 0.004$; $p = 0.41$). ***F***, Same as E at DIV8–10 ($n = 299$ neurons). Line represents linear regression fit ($r = 0.002$; $p = 0.48$). ***G***, Same as E at DIV21–22 ($n = 314$ neurons). Line represents linear regression fit ($r = 0.001$; $p = 0.50$).

potential E_{Cl} equals the GABA reversal potential and used the Nernst equation to determine neuronal chloride concentrations:

$$E_{cl} = -\frac{RT}{zF} ln \frac{[Cl^-]_o}{[Cl^-]_i} = -0.0263 ln \frac{[Cl^-]_o}{[Cl^-]_i} \quad (2)$$

(with $[Cl^-]_o$ = 136.6 mM in ACSF) to convert the measured reversal potentials to estimated $[Cl^-]_i$. We are aware that $GABA_A$ channels are also permeable for HCO_3^- ions (Bormann et al., 1987; Kaila et al., 1993; Kaila, 1994). By assuming that E_{Cl} equals the GABA reversal potential, we will slightly overestimate $[Cl^-]_i$.

Statistical analysis

Statistical analysis was performed with Prism 9 (GraphPad). Normality was tested using Shapiro–Wilk tests. For unpaired samples statistical significance was evaluated using the unpaired Student's *t* test (*t* test) for normally distributed data points, or the nonparametric Mann–Whitney (MW) test otherwise. A one-way ANOVA [or the Kruskal–Wallis (KW) test for non-normal distributions] was used when more than two groups were compared. Cumulative distributions were tested with the Kolmogorov–Smirnov (KS) test. Simple linear regression analysis was used to test whether FRET ratios were influenced by the depth of the soma in the slice.

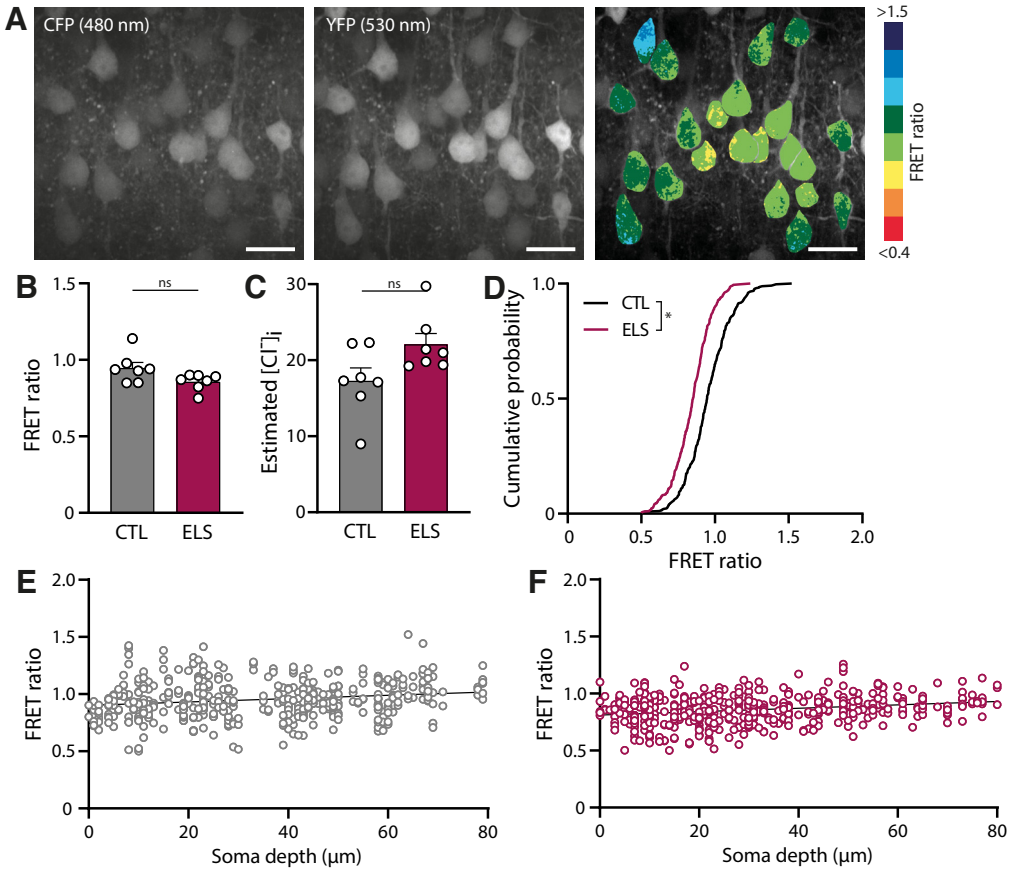

Figure 4. Higher $[Cl^-]_i$ in L2/3 cells in mPFC slices from mice that experienced early life stress. ***A***, Two-photon image of layer 2/3 neurons of the medial PFC of an acute slice of a P9 SClm mouse. Shown is the CFP and YFP fluorescence, and the corresponding FRET ratios. Individual cells are color-coded to their FRET ratios. Scale bar: 20 μm. ***B***, Average FRET ratios from control mice and from mice after ELS. Data from seven mice in both groups ($p = 0.55$, *t* test). The average FRET ratios were significantly lower in the ELS condition when analyzed per slice ($p < 0.01$, *t* test) or per cell ($p < 0.0001$, MW test; data not shown). ***C***, Average estimated $[Cl^-]_i$ as calculated from the FRET ratios in B ($p = 0.07$, MW test). ***D***, Cumulative distribution of individual FRET ratios in slices from control and ELS mice. For each mouse 50 cells were randomly selected, making a total of 350 plotted cells per condition ($p < 0.001$; KS test). ***E***, Individual FRET ratios plotted against soma depth in slices from control mice ($n = 443$ neurons). Line represents linear regression fit ($r = 0.035$; $p < 0.0001$). ***F***, Same as ***E*** for slices from mice after ELS ($n = 470$ neurons). Line represents linear regression fit ($r = 0.058$; $p < 0.0001$).

$p < 0.05$ was considered significant. All data are presented as mean ± SEM.

Results

Two-photon imaging of $[Cl^-]_i$

To quantify the neuronal chloride concentration, SClm expression was targeted to pyramidal neurons by crossing SuperClomeleon$^{lox/-}$ mice (Rahmati et al., 2021) with transgenic mice in which Cre recombinase expression was driven by the calcium/calmodulin-dependent protein kinase II α (CamKIIα) promoter (Tsien et al., 1996; Casanova et al., 2001). CaMKIIα is mostly expressed by excitatory neurons (Sík et al., 1998) and by some glia cells (Pylayeva-Gupta, 2011). In our slices from young SClm mice, we observed many pyramidal neurons in the hippocampus and prefrontal cortex expressing the SClm sensor (Fig. 1*A*). ~35% of the neurons in the adult cortex and ~70% of the neurons in the adult hippocampus express CamKIIα (Wang et al., 2013). In our slices, the fraction of SClm cells is expected to be slightly lower, because CamKIIα expression still increases between P3 and P15 (Casanova et al., 2001).

The optogenetic SClm sensor consists of two fluorescent proteins, Cerulean (CFP mutant) and Topaz (YFP mutant), joined by a flexible linker (Fig. 1*B*). Binding of chloride to YFP reduces the FRET from the donor CFP to the YFP acceptor (Grimley et al., 2013; Arosio and Ratto, 2014). We used two-photon fluorescence microscopy to measure the 530 nm/480 nm (YFP/CFP) emission ratio (hereafter: FRET ratio) of individual cells. We calibrated measured FRET ratios against different $[Cl^-]_i$ using a combination of perforated patch recordings and ionophore treatment (Fig. 1*C*,*D*; for details, see Materials and Methods). Fitting this curve with Equation 1 yielded a K_d value of 24.6 mM (Fig. 1*D*), which is in good agreement with previous reports (Grimley et al., 2013; Rahmati et al., 2021). The range of values for R_{max} measured in

different calibration experiments was between 1.30 and 1.82. R_{min} ranged between 0.38 and 0.48. We used this fit to convert measured FRET ratios into $[Cl^-]_i$, for all our experiments, but we are aware that these should be considered reasonable estimates of the actual intracellular chloride levels at best.

Acute manipulation of $[Cl^-]_i$ in brain slices

To assess the responsiveness of the SCIm sensor to changes in intracellular chloride, we patched a pyramidal neuron in an acute hippocampal slice with a high concentration of chloride in the patch pipette, while monitoring changes in SCIm FRET ratios. The FRET ratio in the patched cell changed immediately after break-in because of the rapid influx of chloride (Fig. 2*A*,*B*). This decrease in FRET ratio was not observed in neighboring cells in the same field of view (Fig. 2*C*). In a separate set of experiments, we monitored changes in FRET ratios during wash-in of muscimol, a specific $GABA_A$ receptor agonist. As $GABA_A$ receptors are chloride channels, activation of $GABA_A$ receptors will induce influx of chloride ions, and therefore result in an increase in $[Cl^-]_i$. We observed a rapid 20% decrease in FRET ratio (indicating a 5–10 mM change in $[Cl^-]_i$) on administration of muscimol, caused by the cellular influx of chloride (Fig. 2*D*,*E*). These experiments demonstrate that the SCIm sensor reliably reports rapid changes in neuronal $[Cl^-]_i$ within the physiological range.

Development of neuronal $[Cl^-]_i$ levels in organotypic cultures

Next, we imaged neuronal $[Cl^-]_i$ levels in cultured hippocampal slices at different developmental stages. FRET ratios were determined at DIV2–3, DIV8–10, and DIV20–21 (Fig. 3*A*). We observed a clear increase in FRET ratios, corresponding with a decrease in $[Cl^-]_i$, between DIV2–3 and DIV8–10 (Fig. 3*B*,*C*). Although the average FRET ratio was very similar at DIV20–21 and DIV8–10, the fraction of cells with high FRET ratios appeared larger at DIV20–21 (Fig. 3*D*), suggesting that chloride levels in some neurons were still decreasing at this age. FRET ratios were not dependent on the depth of the somata in the slice (Fig. 3*E–G*). This indicates that cell-to-cell differences were not because of their location in the slice and we also confirmed that FRET values are independent of fluorescence intensity (data not shown). Our results show that the GABA shift continues in organotypic hippocampal cultures during the first two weeks *in vitro*.

Early life stress elevates neuronal $[Cl^-]_i$ at P9

We then used the SCIm sensor to detect changes in intracellular chloride levels over development in the prefrontal cortex in young mice after ELS. To induce ELS in young mice, we provided a limited amount of nesting and bedding material to the mothers between P2 and P9, resulting in fragmented and unpredictable maternal care (Rice et al., 2008; Naninck et al., 2015; Karst et al., 2020). To examine whether this early life experience affected chloride maturation in the young pups, we measured FRET ratios in layer 2/3 neurons in acute slices from the mPFC from control and ELS male mice at P9, immediately after the stress period (Fig. 4*A*). In total, 443 and 470 neurons were included in the analysis obtained from seven control and seven ELS mice, respectively. As expected, average $[Cl^-]_i$ levels were higher in mPFC compared with hippocampal pyramidal cells at comparable age [~17.3 mM in P9 mPFC slices (Fig. 4*C*) to ~11.5 mM in DIV2–3 cultured hippocampal slices (Fig. 3*C*)]. This likely reflects the delayed maturation of the PFC compared with the hippocampus (Amadeo et al., 2018; Karst et al., 2019). Average FRET ratios in layer 2/3 pyramidal cells in slices from SCIm mice that experienced ELS were slightly lower compared with control, but this difference was not significant when comparing average FRET ratios per mouse (Fig. 4*B*,*C*). However, when we analyzed the distribution of FRET ratios in individual cells, we observed a significant shift toward more cells with a lower FRET ratio in the ELS condition (Fig. 4*D*). A small dependence of FRET ratio on soma depth was found for both conditions in acute prefrontal slices (Fig. 4*E*,*F*). As this was different from our observations in slice cultures (Fig. 3*E–G*), we suspect it may reflect surface damage from slicing. Together our results show that ELS leads to an increase in neurons with high, immature chloride levels at P9 compared with control mice.

Discussion

In this study, we performed two-photon chloride imaging using the SCIm sensor to determine the time course of chloride maturation in cultured hippocampal slices and to examine alterations of the chloride development in the mPFC by ELS. Previous nonratiometric chemical indicators, including 6-methoxy-N-(3-sulfopropyl)quinolinium (SPQ) and N-(ethoxycarbonylmethyl)-6methoxyquinolinium bromide (MQAE; Illsley and Verkman, 1987; Verkman et al., 1989), have the disadvantage that their fluorescence depends not only on $[Cl^-]_i$, but also on the dye concentration and optical thickness at each location, e.g., depth in the slice or in the brain. Therefore, SPQ and MQAE allow for the assessment of acute changes in $[Cl^-]_i$ within the same neurons (Arosio and Ratto, 2014; Zajac et al., 2020), but cannot be used to study developmental changes which requires comparisons between animals and between slices. The SCIm sensor has an improved affinity for chloride compared with its processor Clomeleon (Berglund et al., 2006), resulting in a more than fourfold improvement in signal-to-noise over Clomeleon (Grimley et al., 2013). Two-photon chloride imaging poses major advantages over perforated patch clamp recordings. Most importantly, chloride imaging allows for assessing of $[Cl^-]_i$ over time in multiple neurons simultaneously in a noninvasive manner. One important limitation of the SCIm sensor is its sensitivity to intracellular pH (pH_i; Lodovichi et al., 2022). However, we do not expect large changes in pH_i in our in vitro experiments, and pH_i remains fairly constant during postnatal development (Sulis Sato et al., 2017). Using SCIm, we could directly measure changes in $[Cl^-]_i$ when we loaded 70 mM chloride into a neuron via the patch pipette and after addition of a $GABA_A$ receptor agonist. This demonstrates that the SCIm sensor reliably reports changes in intracellular chloride within the

physiological range. Furthermore, we could detect subtle changes in the distribution of individual $[Cl^-]_i$ levels within the pyramidal cell population during normal and disturbed postnatal development. Subtle changes at the population level are physiologically relevant and would have been hard to pick up otherwise.

Although the advantages of direct chloride imaging using the SCIm sensor are numerous, we found that the conversion of FRET ratios to absolute values of intracellular chloride concentrations was not very robust. In our hands, calibration using ionophores and varying extracellular chloride concentrations gave variable results. Variable FRET ratios, especially in the physiological range (5–10 mM), hampered reliable calibration to $[Cl^-]_i$. Compared with our cultured slices, cultured primary neurons are better accessible for ionophores. Cultured neurons are therefore expected to respond more consistently to changes in extracellular chloride levels during ionophore calibration (Grimley et al., 2013; Boffi et al., 2018), and this method is more unpredictable in cultured slices. In addition, strong regulation of intracellular chloride levels (Kaila et al., 2014; Rahmati et al., 2021) and variable resilience of neurons to the harsh calibration conditions may have hampered the calibration procedure in our slices. We therefore resorted to using perforated patch clamp and inferred chloride concentrations from the reversal potential of $GABA_A$ currents. Although our calibration curve was in good agreement with previous reports (Grimley et al., 2013; Rahmati et al., 2021), we noticed that small alterations in the fit strongly affect chloride level estimates. We therefore conclude that the SCIm sensor is an excellent tool to measure relative changes in $[Cl^-]_i$ which are physiological relevant, but that conversion to absolute chloride concentrations should be interpreted with care. In our view, this disadvantage does not outweigh the significant benefits of using the SCIm sensor to detect changes in neuronal chloride levels over time and between conditions. In recent years, genetically encoded fluorescent sensors have been developed which enable imaging of different molecules. Live imaging studies using these sensors, most prominently of intracellular calcium, have made great contributions to our understanding of intracellular and intercellular signaling (Day-Cooney et al., 2022; Dong et al., 2022), despite the fact that calibration of most of these sensors to absolute concentrations remains notoriously difficult. We hope that current and future chloride sensors (Zajac et al., 2020; Lodovichi et al., 2022) will make a similar impact on our understanding of chloride homeostasis.

Using the SCIm sensor, we have monitored the developmental decrease in neuronal chloride levels in organotypic hippocampal cultures from SCIm mice. The SCIm sensor proved more sensitive than its precursor Clomeleon, which was previously used to determine chloride maturation in cultured neurons and in an in vitro epilepsy model (Kuner and Augustine, 2000; Dzhala and Staley, 2021). With the SCIm sensor we could discern that neuronal chloride levels in our cultured slices show a clear reduction between DIV3 and DIV9 (equivalent to the second postnatal week *in vivo*), and that in some pyramidal cells chloride levels continue to decrease until DIV22. The large cell-to-cell differences that we observe have been previously reported (Stein et al., 2004; Yamada et al., 2004; Dzhala et al., 2012; Kirmse et al., 2015; Sulis Sato et al., 2017). The estimated $[Cl^-]_i$ values in our developing cultured slices are in good agreement with previous estimates in cultured hippocampal neurons (Kuner and Augustine, 2000; Tyzio et al., 2007), and acute hippocampal slices (Staley and Proctor, 1999; Tyzio et al., 2007). A recent study using LSSmClopHensor chloride sensor in the visual cortex *in vivo* (Sulis Sato et al., 2017) also showed a rapid reduction in $[Cl^-]_i$ during the first postnatal week, followed by a slow further decrease to mature levels.

Brain development is strongly influenced by external factors and early life experiences (Hensch, 2004; Miguel et al., 2019). Here, we used ELS, an established model to interfere with early brain development with long-lasting consequences for psychopathological risks later in life (Teicher et al., 2016; Joëls et al., 2018; Bachiller et al., 2022; Catale et al., 2022). We used SCIm to detect possible alterations in chloride maturation in the mPFC. We observed that ELS results in a shift toward higher (i.e., immature) chloride levels in individual layer 2/3 cells in the mPFC. This suggests that ELS delays the GABA shift in SCIm mice, but we did not examine chloride levels at older ages. Our results are in line with previous reports showing a delayed GABA shift in hippocampal neurons after prenatal maternal restraint stress and when newborn pups were repeatedly separated from their mother (Veerawatananan et al., 2016; Furukawa et al., 2017; Hu et al., 2017). However, the effect on the GABA shift can be very sensitive to the type and timing of stress, and a different maternal separation paradigm resulted in an advance of the hippocampal GABA shift (Galanopoulou, 2008). Using the same ELS paradigm in C57/BL6 mice, we previously reported accelerated maturation of synaptic currents in layer 2/3 mPFC pyramidal cells (Karst et al., 2020), and decreased $[Cl^-]_i$ levels in young pups after ELS (Karst et al., 2019). Although we used the same stress paradigm and mice were housed in the same facility, the effect of ELS on $[Cl^-]_i$ was remarkably different between the SCIm and WT mice. Chloride homeostasis is highly regulated and affected by many intracellular factors including the chloride buffering capacity (Rahmati et al., 2021), and we cannot exclude that the permanent presence of a chloride sensor induces subtle changes in the regulation of chloride homeostasis in neurons in SCIm mice. However, the $[Cl^-]_i$ we report here in SCIm (unstressed) controls (17.3 mM) was comparable to the chloride concentration that was previously measured by perforated patch in WT C57/BL6 control mice (18.8 mM; H. Karst, unpublished observations), suggesting that the difference cannot be explained by a difference in baseline chloride levels. The response to stress can differ substantially between mouse strains and C57BL/6 mice appear more resilient to stress in comparison to other strains (Murthy and Gould, 2018). Unfortunately, we did not directly compare the two mouse lines. A difference in ELS response may indicate a difference in genetic predisposition with possible consequences for stress responses and stress-related behavior (McIlwrick et al., 2016; Teicher et al., 2016; Joëls et al., 2018). The poor breeding performance of SCIm mice may also reflect

differences in stress response compared with C57BL/6 mice. Our results underscore that the developmental chloride trajectory appears incredibly sensitive to environmental factors and may differ between mouse lines. We advise to take these differences into account in behavioral experiments.

Our data demonstrate that the high sensitivity of the SCIm sensor at relevant chloride concentrations allows detecting physiological alterations in neuronal chloride levels during normal and altered postnatal development. Although we also found some limitations, our study underscores that two-photon chloride imaging is a powerful technique to further illuminate the role of chloride signaling in the brain.

References

Amadeo A, Coatti A, Aracri P, Ascagni M, Iannantuoni D, Modena D, Carraresi L, Brusco S, Meneghini S, Arcangeli A, Pasini ME, Becchetti A (2018) Postnatal changes in K+/Cl- cotransporter-2 expression in the forebrain of mice bearing a mutant nicotinic subunit linked to sleep-related epilepsy alida. Neuroscience 386:91–107.

Arosio D, Ratto GM (2014) Twenty years of fluorescence imaging of intracellular chloride. Front Cell Neurosci 8:1–12.

Arosio D, Ricci F, Marchetti L, Gualdani R, Albertazzi L, Beltram F (2010) Simultaneous intracellular chloride and pH measurements using a GFP-based sensor. Nat Methods 7:516–518.

Bachiller S, Hidalgo I, Garcia MG, Boza-Serrano A, Paulus A, Denis Q, Haikal C, Manouchehrian O, Klementieva O, Li JY, Pronk CJ, Gouras GK, Deierborg T (2022) Early-life stress elicits peripheral and brain immune activation differently in wild type and 5xFAD mice in a sex-specific manner. J Neuroinflammation 19:151.

Ben-Ari Y, Gaiarsa J, Tyzio R, Khazipov R (2007) GABA: a pioneer transmitter that excites immature neurons and generates primitive oscillations. Physiol Rev 87:1215–1284.

Berglund K, Schleich W, Krieger P, Loo LS, Wang D, Cant NB, Feng G, Augustine GJ, Kuner T (2006) Imaging synaptic inhibition in transgenic mice expressing the chloride indicator, Clomeleon. Brain Cell Biol 35:207–228.

Boffi JC, Knabbe J, Kaiser M, Kuner T (2018) KCC2-dependent steady-state intracellular chloride concentration and ph in cortical layer 2/3 neurons of anesthetized and awake mice. Front Cell Neurosci 12:1–14.

Bormann J, Hamill OP, Sakmann B (1987) Mechanism of anion permeation through channels gated by glycine and gamma-aminobutyric acid in mouse cultured spinal neurones. J Physiol 385:243–286.

Casanova E, Fehsenfeld S, Mantamadiotis T, Lemberger T, Greiner E, Stewart AF, Schütz G (2001) A CamKIIalpha iCre BAC allows brain-specific gene inactivation. Genesis 31:37–42.

Catale C, Martini A, Piscitelli RM, Senzasono B, Lo IL, Mercuri NB, Guatteo E, Carola V (2022) Early-life social stress induces permanent alterations in plasticity and perineuronal nets in the mouse anterior cingulate cortex. Eur J Neurosci 56:5763–5783.

Day-Cooney J, Dalangin R, Zhong H, Mao T (2022) Genetically encoded fluorescent sensors for imaging neuronal dynamics in vivo. J Neurochem 1–25. Available at https://doi.org/10.1111/jnc.15608.

Dong C, Zheng Y, Long-Iyer K, Wright EC, Li Y, Tian L (2022) Fluorescence imaging of neural activity, neurochemical dynamics, and drug-specific receptor conformation with genetically encoded sensors. Annu Rev Neurosci 45:273–294.

Dzhala VI, Staley KJ (2021) Kcc2 chloride transport contributes to the termination of ictal epileptiform activity. eNeuro 8: ENEURO.0208-20.2020.

Dzhala V, Valeeva G, Glykys J, Khazipov R, Staley K (2012) Traumatic alterations in GABA signaling disrupt hippocampal network activity in the developing brain. J Neurosci 32:4017–4031.

Furukawa M, Tsukahara T, Tomita K, Iwai H, Sonomura T, Miyawaki S, Sato T (2017) Neonatal maternal separation delays the GABA excitatory-to-inhibitory functional switch by inhibiting KCC2 expression. Biochem Biophys Res Commun 493:1243–1249.

Galanopoulou AS (2008) Dissociated gender-specific effects of recurrent seizures on GABA signaling in CA1 pyramidal neurons: role of GABA(A) receptors. J Neurosci 28:1557–1567.

Glykys J, Dzhala VI, Kuchibhotla KV, Feng G, Kuner T, Augustine G, Bacskai B, Staley K (2009) Differences in cortical versus subcortical GABAergic signaling: a candidate mechanism of electroclinical uncoupling of neonatal seizures. Neuron 63:657–672.

Grimley J, Li L, Wang W, Wen L, Beese L, Hellinga H, Augustine G (2013) Visualization of synaptic inhibition with an optogenetic sensor developed by cell-free protein engineering automation. J Neurosci 33:16297–16309.

Hensch TK (2004) Critical period regulation. Annu Rev Neurosci 27:549–579.

Hu D, Yu ZL, Zhang Y, Han Y, Zhang W, Lu L, Shi J (2017) Bumetanide treatment during early development rescues maternal separation-induced susceptibility to stress. Sci Rep 7:11878.

Illsley NP, Verkman AS (1987) Membrane chloride transport measured using a chloride-sensitive fluorescent probe. Biochemistry 26:1215–1219.

Ishikawa J, Nishimura R, Ishikawa A (2015) Early-life stress induces anxiety-like behaviors and activity imbalances in the medial prefrontal cortex and amygdala in adult rats. Eur J Neurosci 41:442–453.

Joëls M, Karst H, Sarabdjitsingh RA (2018) The stressed brain of humans and rodents. Acta Physiol (Oxf) 223:e13066.

Kaila K (1994) Ionic basis of GABAA receptor channel function in the nervous system. Prog Neurobiol 42:489–537.

Kaila K, Voipio J, Paalasmaa P, Pasternack M, Deisz RA (1993) The role of bicarbonate in GABAA receptor-mediated IPSPs of rat neocortical neurones. J Physiol 464:273–289.

Kaila K, Price TJ, Payne JA, Puskarjov M, Voipio J (2014) Cation-chloride cotransporters in neuronal development, plasticity and disease. Nat Rev Neurosci 15:637–654.

Karst H, van Mourik LI, Joëls M (2019) Early life stress in mice causes a change in the excitation-inhibition balance in prefrontal cortex neurons during development. 409.03 Neuroscience 2019 Abstracts. Chicago, IL: Society for Neuroscience.

Karst H, Sarabdjitsingh RA, van der Weerd N, Feenstra E, Damsteegt R, Joëls M (2020) Age-dependent shift in spontaneous excitation-inhibition balance of infralimbic prefrontal layer II/III neurons is accelerated by early life stress, independent of forebrain mineralocorticoid receptor expression. Neuropharmacology 180:108294.

Kirmse K, Kummer M, Kovalchuk Y, Witte OW, Garaschuk O, Holthoff K (2015) GABA depolarizes immature neurons and inhibits network activity in the neonatal neocortex in vivo. Nat Commun 6:7750.

Kuner T, Augustine GJ (2000) A genetically encoded ratiometric indicator for chloride. Neuron 27:447–459.

Lodovichi C, Ratto GM, Trevelyan AJ, Arosio D (2022) Genetically encoded sensors for chloride concentration. J Neurosci Methods 368:109455.

Lohmann C, Kessels HW (2014) The developmental stages of synaptic plasticity. J Physiol 592:13–31.

McIlwrick S, Rechenberg A, Matthes M, Burgstaller J, Chen A, Schwarzbauer T, Touma C (2016) Genetic predisposition for high stress reactivity amplifies effects of early-life adversity. Psychoneuroendocrinology 70:85–97.

McKlveen JM, Myers B, Herman JP (2015) The medial prefrontal cortex: coordinator of autonomic, neuroendocrine and behavioural responses to stress. J Neuroendocrinol 27:446–456.

Miguel P, Pereira L, Silveira P, Meaney M (2019) Early environmental influences on the development of children's brain structure and function. Dev Med Child Neurol 61:1127–1133.

Murata Y, Colonnese MT (2020) GABAergic interneurons excite neonatal hippocampus in vivo. Sci Adv 6:eaba1430.
Murthy S, Gould E (2018) Early life stress in rodents: animal models of illness or resilience? Front Behav Neurosci 12:1–5.
Naninck EFG, Hoeijmakers L, Kakava-Georgiadou N, Meesters A, Lazic SE, Lucassen PJ, Korosi A (2015) Chronic early life stress alters developmental and adult neurogenesis and impairs cognitive function in mice. Hippocampus 25:309–328.
Peerboom C, Wierenga CJ (2021) The postnatal GABA shift: a developmental perspective. Neurosci Biobehav Rev 124:179–192.
Pressman B, Fahim M (1982) Pharmacology and toxicology of the monovalent carboxylic ionophores. Annu Rev Pharmacol Toxicol 22:465–490.
Pylayeva-Gupta Y (2011) Activity-dependent validation of excitatory vs. inhibitory synapses by neuroligin-1 vs. neuroligin-2. Bone 23:1–7.
Rahmati N, Normoyle KP, Glykys J, Dzhala VI, Lillis KP, Kahle KT, Raiyyani R, Jacob T, Staley KJ (2021) Unique actions of gaba arising from cytoplasmic chloride microdomains. J Neurosci 41:4967–4975.
Rice CJ, Sandman CA, Lenjavi MR, Baram TZ (2008) A novel mouse model for acute and long-lasting consequences of early life stress. Endocrinology 149:4892–4900.
Rivera C, Voipio J, Payne JA, Ruusuvuori E, Lahtinen H, Lamsa K, Pirvola U, Saarma M, Kaila K (1999) The K+/Cl- co-transporter KCC2 renders GABA hyperpolarizing during neuronal maturation. Nature 397:251–255.
Romo-Parra H, Treviño M, Heinemann U, Gutiérrez R (2008) GABA actions in hippocampal area CA3 during postnatal development: differential shift from depolarizing to hyperpolarizing in somatic and dendritic compartments. J Neurophysiol 99:1523–1534.
Sernagor E, Chabrol F, Bony G, Cancedda L (2010) Gabaergic control of neurite outgrowth and remodeling during development and adult neurogenesis: general rules and differences in diverse systems. Front Cell Neurosci 4:1–11.
Sík A, Hájos N, Gulácsi A, Mody I, Freund TF (1998) The absence of a major Ca2+ signaling pathway in GABAergic neurons of the hippocampus. Proc Natl Acad Sci U S A 95:3245–3250.
Staley KJ, Proctor WR (1999) Modulation of mammalian dendritic GABA(A) receptor function by the kinetics of Cl- and HCO3- transport. J Physiol 519:693–712.
Stein V, Hermans-Borgmeyer I, Jentsch TJ, Hübner CA (2004) Expression of the KCl cotransporter KCC2 parallels neuronal maturation and the emergence of low intracellular chloride. J Comp Neurol 468:57–64.
Stoppini A, Buchs PA, Müller D (1991) A simple method for organotypic cultures of nervous tissue. J Neurosci Methods 37:173–182.
Sulis Sato S, Artoni P, Landi S, Cozzolino O, Parra R, Pracucci E, Trovato F, Szczurkowska J, Luin S, Arosio D, Beltram F, Cancedda L, Kaila K, Ratto GGM (2017) Simultaneous two-photon imaging of intracellular chloride concentration and pH in mouse pyramidal neurons in vivo. Proc Natl Acad Sci U S A 114:201702861.
Teicher MH, Samson JA, Anderson CM, Ohashi K (2016) The effects of childhood maltreatment on brain structure, function and connectivity. Nat Rev Neurosci 17:652–666.
Tsien JZ, Chen DF, Gerber D, Tom C, Mercer EH, Anderson DJ, Mayford M, Kandel ER, Tonegawa S (1996) Subregion- and cell type-restricted gene knockout in mouse brain. Cell 87:1317–1326.
Tyzio R, Holmes GL, Ben-Ari Y, Khazipov R (2007) Timing of the developmental switch in GABA(A) mediated signaling from excitation to inhibition in CA3 rat hippocampus using gramicidin perforated patch and extracellular recordings. Epilepsia 48:96–105.
Veerawatananan B, Surakul P, Chutabhakdikul N (2016) Maternal restraint stress delays maturation of cation-chloride cotransporters and GABAA receptor subunits in the hippocampus of rat pups at puberty. Neurobiol Stress 3:1–7.
Verkman AS, Sellers MC, Chao AC, Leung T, Ketcham R (1989) Synthesis and characterization of improved chloride-sensitive fluorescent indicators for biological applications. Anal Biochem 178:355–361.
Wang BS, Feng L, Liu M, Liu X, Cang J (2013) Environmental enrichment rescues binocular matching of orientation preference in mice that have a precocious critical period. Neuron 80:198–209.
Yamada J, Okabe A, Toyoda H, Kilb W, Luhmann H, Fukuda A (2004) Cl− uptake promoting depolarizing GABA actions in immature rat neocortical neurones is mediated by NKCC1. J Physiol 557:829–841.
Zajac M, Chakraborty K, Saha S, Mahadevan V, Infield DT, Accardi A, Qiu Z, Krishnan Y (2020) What biologists want from their chloride reporters - A conversation between chemists and biologists. J Cell Sci 133:jcs240390.